

Photoelectrical Stimulation of Neuronal Cells by an Organic Semiconductor-Electrolyte Interface

Oliya S. Abdullaeva, Matthias Schulz, Frank Balzer, Jürgen Parisi, Arne Luetzen, Karin Dedek, and Manuela Schiek

Langmuir, **Just Accepted Manuscript** • DOI: 10.1021/acs.langmuir.6b02085 • Publication Date (Web): 01 Aug 2016

Downloaded from <http://pubs.acs.org> on August 8, 2016

Just Accepted

“Just Accepted” manuscripts have been peer-reviewed and accepted for publication. They are posted online prior to technical editing, formatting for publication and author proofing. The American Chemical Society provides “Just Accepted” as a free service to the research community to expedite the dissemination of scientific material as soon as possible after acceptance. “Just Accepted” manuscripts appear in full in PDF format accompanied by an HTML abstract. “Just Accepted” manuscripts have been fully peer reviewed, but should not be considered the official version of record. They are accessible to all readers and citable by the Digital Object Identifier (DOI®). “Just Accepted” is an optional service offered to authors. Therefore, the “Just Accepted” Web site may not include all articles that will be published in the journal. After a manuscript is technically edited and formatted, it will be removed from the “Just Accepted” Web site and published as an ASAP article. Note that technical editing may introduce minor changes to the manuscript text and/or graphics which could affect content, and all legal disclaimers and ethical guidelines that apply to the journal pertain. ACS cannot be held responsible for errors or consequences arising from the use of information contained in these “Just Accepted” manuscripts.



Photoelectrical Stimulation of Neuronal Cells by an Organic Semiconductor-Electrolyte Interface

Oliya S. Abdullaeva,[†] Matthias Schulz,[‡] Frank Balzer,[¶] Jürgen Parisi,[†] Arne Lützen,[‡] Karin Dedek,[§] and Manuela Schiek^{*,†}

Energy and Semiconductor Research Laboratory, Institute of Physics, University of Oldenburg, D-26111 Oldenburg, Germany, Kekulé Institute of Organic Chemistry and Biochemistry, Rheinische-Friedrich-Wilhelms-University of Bonn, Gerhard-Domagk-Str. 1, D-53121 Bonn, Germany, Mads Clausen Institute, University of Southern Denmark, Alsion 2, DK-6400 Sønderborg, Denmark, and Neurosensorics, Institute for Biology and Environmental Sciences, University of Oldenburg, D-26111 Oldenburg, Germany

E-mail: manuela.schiek@uni-oldenburg.de

Abstract

As a step towards the realization of neuro-prosthetics for vision restoration, we follow an electrophysiological patch-clamp approach to study the fundamental photoelectrical stimulation mechanism of neuronal model cells by an organic semiconductor-electrolyte interface. Our photoactive layer consisting of an anilino-squaraine donor blended with a fullerene acceptor is supporting the growth of the neuronal model cell line (N2A cells) without an adhesion layer on it, and is not impairing cell viability. The transient photocurrent signal upon illumination from the semiconductor-electrolyte layer is

*To whom correspondence should be addressed

[†]University of Oldenburg, Physics

[‡]University of Bonn

[¶]SDU Sønderborg

[§]University of Oldenburg, Biology

1
2
3 able to trigger a passive response of the neuronal cells under physiological conditions
4
5 via a capacitive coupling mechanism. We study the dynamics of the capacitive trans-
6
7 membrane currents by patch-clamp recordings and compare them to the dynamics of
8
9 the photocurrent signal and its spectral responsivity. Furthermore, we characterize the
10
11 morphology of the semiconductor-electrolyte interface by atomic force microscopy, and
12
13 study the stability of the interface in dark and under illuminated conditions.
14

15 **Version:** July 26, 2016, 13:44
16
17
18
19

20 Introduction

21

22
23 Research on the realization of neuroelectronic interfaces between silicon chips and nerve cells ¹
24 as well as organic bio-electronic devices ²⁻⁴ emerged together with the advances in semicon-
25 ductor technology and neurobiology. Apart from gaining insight into fundamental signaling
26 principles from electronic devices to living systems, such kind of research can ultimately pro-
27 vide prosthetic therapy tools. For instance, in many blindness-causing diseases, photorecep-
28 tors degenerate whereas second-order and projecting neurons are largely unaffected. Thus,
29 one promising avenue to restore vision in affected patients is to develop artificial photore-
30 ceptors for retinal prosthetic devices using light directed electrical neuronal stimulation ^{5,6}.
31 Alternative approaches are chemical neuronal stimulation via voltage-controlled devices for
32 trafficking of the neurotransmitter glutamate ⁷, or "device-less" photochemical stimulation
33 via a photopharmacological ⁸ or an optochemical genetic strategy ⁹. Regarding the photo-
34 electrical stimulation, it has already been demonstrated that the semiconducting polymer
35 poly-3-hexyl-thiophene (P3HT) under physiological conditions was able to trigger neuronal
36 action potentials in primary cultures of hippocampal neurons ¹⁰, explanted rat retinas ¹¹, and
37 embryonic chick retinas ¹² via a photoelectrical stimulation mechanism, or induced opening
38 of voltage-gated ion channels in neuronal cells via a photothermal activation mechanism ¹³.
39
40
41
42
43
44
45
46
47
48
49
50
51
52
53
54

55 The advantages of employing organic photoconductors instead of inorganic electronic
56 materials in retinal prosthetic devices would include the redundancy of a camera and an
57
58
59
60

1
2
3 external power supply. In general, the increased (mechanical) compatibility of organic soft
4 matter with tissue is a major benefit¹⁴. Van-der-Waals bound soft organic matter facil-
5 itates intimate interfaces with aqueous electrolytes due to the absence of dangling bonds
6 and surface oxides¹⁵. Furthermore, organic matter can mediate ion conduction allowing
7 for communication with biological systems, where ion fluxes are of major importance. In
8 addition, organic molecules can easily be chemically modified to tune the required func-
9 tionality of the material, which holds in particular true for small molecular compounds.
10 Thus, we have chosen a representative from the class of squaraine dyes for our studies: 2,4-
11 bis[4-(*N,N*-diisobutylamino)-2,6-dihydroxyphenyl]squaraine, shortly named SQIB, Fig. 1(a).
12 Squaraine dyes are characterized by their unique aromatic four-membered ring system and
13 their zwitterionic nature, making them environmentally stable and facilitating intense ab-
14 sorption within the deep-red of the visible light spectrum¹⁶. In the past, they have been
15 prominent as xerographic materials¹⁷, nowadays, they are employed as light-harvesting com-
16 pounds in photovoltaic devices^{18–20} among other technologically relevant applications^{21,22}.
17
18
19
20
21
22
23
24
25
26
27
28
29
30
31

32 We prepare the photoactive layer by spin-casting SQIB blended with the conventional
33 fullerene acceptor [6.6]phenyl-C₆₁-butyric-acid-methyl ester (PCBM) on indium tin oxide
34 (ITO) coated glass substrates followed by thermal annealing. As typical for molecular semi-
35 conductors, the SQIB crystallizes upon annealing and forms a textured film with two distinct
36 structural motifs, which are referred to as ferns and platelets later on. The surface texture
37 contributes to good adhesion of the non-photoactive murine neuroblastoma *neuro-2a* (N2A)
38 cells, which we grow as neuronal model system. The cells are even able to adhere to the
39 photoactive layer without a protein adhesion layer. This ability is considered as being advan-
40 tageous for neuroelectronic interfacing²³. Investigation of the morphological stability of the
41 photoactive layer/physiological electrolyte junction in dark and under illuminated conditions
42 by atomic force microscopy (AFM) reveals long-term stability in dark, but degradation after
43 a few days under continuous illumination.
44
45
46
47
48
49
50
51
52
53
54
55

56 Upon pulsed illumination of the active layer/electrolyte junction, a transient displace-
57
58
59
60

1
2
3
4
5
6
7
8
9
10
11
12
13
14
15
16
17
18
19
20
21
22
23
24
25
26
27
28
29
30
31
32
33
34
35
36
37
38
39
40
41
42
43
44
45
46
47
48
49
50
51
52
53
54
55
56
57
58
59
60

ment current can be measured within the electrolyte^{11,24}. Electrophysiological patch-clamp recordings on the N2A cells under physiological conditions show that this extracellular electrical stimulus induces a change in membrane potential, resulting in capacitive transmembrane currents. The electrical coupling, however, is not strong enough to activate a reversible opening of the voltage-gated ion channels, which classifies the desired, active response of a neuronal cell. Since the photoconductor-electrolyte junction is determining the coupling, we focus on characterizing the morphological and opto-electronical properties of the junction. Spatially resolved absorption spectra allow to assign the signatures within the absorption spectra to the two different morphological features. Recording the external quantum efficiency (EQE) across the junction of electrically contacted samples shows a strong correlation of absorbance and photocurrent density. Studying the transient photocurrent signal and the corresponding transmembrane currents spatially resolved with respect to the two different morphological features reveals only a weak local variation.

Materials and Methods

Synthesis of 2,4-bis[4-(*N,N*-diisobutylamino)-2,6-dihydroxyphenyl]-squaraine

Synthesis was done by a modified version of the previously reported protocol²⁵. Under argon atmosphere, a mixture of phloroglucinol (1.26 g, 10 mmol), diisobutylamine (1.9 mL, 11 mmol) and 40 mL of 1-butanol:toluene (ratio 1:3) was refluxed for 16 h with azeotropic distillation of water. After cooling to room temperature, the volatiles were evaporated under reduced pressure. The resulting reddish-brown crude product was purified by column chromatography on silica gel eluting with cyclohexane/acetone (volume ratio 4:1 to 2:1). This gave the intermediate 1,3-dihydroxy-5-(diisobutyl)aminobenzene (1.15 g, 4.8 mmol, 48% yield assuming pure product) as a viscous brown liquid. Subsequently, the intermediate aniline was refluxed with squaric acid (0.27 g, 2.4 mmol) and 30 mL of a mixture of 1-

1
2
3 propanol:toluene (volume ratio 1:1) for 16 h under argon atmosphere with azeotropic distilla-
4 tion of water. The deep blue reaction mixture was slowly cooled down to room temperature
5 and stored at 2 °C overnight to promote crystallization. The green precipitate was filtered
6 off and washed with methanol. The crude product was purified by recrystallization from
7 methanol:dichloromethane (volume ratio 2:1) to yield the product (958 mg, 1.7 mmol, 72 %
8 yield) as golden-green crystals with metallic luster (total yield 35 %).

9
10
11 $^1\text{H-NMR}$: (500 MHz, CDCl_3 , RT) δ [ppm] = 10.96 (s, 4 H, OH), 5.80 (s, 4 H, H_{arom}),
12 3.23 (d, $^3\text{J}=7.5$ Hz, 8 H, NCH_2), 2.12 (m, 4 H, NCH_2CH), 0.92 (d, $^3\text{J}=6.7$ Hz, 24 H, CH_3).
13

14
15
16 $^{13}\text{C-NMR}$: (126 MHz, CDCl_3 , RT) δ [ppm] = 181.5, 162.7, 161.4, 158.3, 102.6, 94.5, 60.5,
17 27.8, 20.3.
18

19
20 MS: (EI, 70 eV) (250 °C) m/z (%) = 552.4 (56) $[\text{M}]^+$, 509.3 (100) $[\text{M}-\text{C}_3\text{H}_7]^+$.
21

22
23 HRMS (EI) calcd for $\text{C}_{32}\text{H}_{44}\text{N}_2\text{O}_6$ $[\text{M}]^+$: 552.311 99 amu; found: 552.311 97 amu.
24

25
26 Elemental analysis: calcd for $\text{C}_{32}\text{H}_{44}\text{N}_2\text{O}_6 \cdot 0.02 \text{CH}_2\text{Cl}_2$: C 69.37, H 8.01, N 5.05; found:
27 H 69.00, H 8.21, N 5.02.
28
29
30
31
32
33

34 Photoactive layer sample preparation

35
36 A 6 mg/mL solution of 2,4-bis[4-(*N,N*-diisobutylamino)-2,6-dihydroxyphenyl]squaraine (SQIB)
37 in chloroform (Sigma-Aldrich, stabilized with amylene) was freshly prepared. After stir-
38 ring overnight, 6 mg/mL phenyl-C61-butyric-acid-methyl ester (PCBM, Solenne) were added
39 resulting a SQIB:PCBM solution with 1:1 blend ratio by weight, which was also stirred
40 overnight. Indium tin oxide (ITO) layers supported on glass substrates (10 mm \times 10 mm or
41 25 mm \times 25 mm, 30 to 40 Ω) were cleaned with distilled water, blow-dried with nitrogen, and
42 exposed to oxygen plasma for 10 min. The SQIB:PCBM solution was spincoated onto the
43 ITO substrates under inert atmosphere at 950 rpm, ramping 0, for 1 s, followed by annealing
44 at 180 °C for 2 h.
45
46
47
48
49
50
51
52
53
54
55
56
57
58
59
60

Cell cultivation and cell counting

Mouse neuroblastoma (N2A) cells were grown in Dulbecco's Modified Eagle Medium (F0455, Biochrom GmbH, Germany), supplemented with 10 % fetal calf serum and L-glutamine. Cells were kept at 37 °C in a 5% CO₂ incubator and were seeded on substrates at a density of 10⁴ cells per well in a 24-well plate. Photoactive layer samples were placed at the bottom of each well with the coated side facing upwards to serve as growth substrate. Cells were recorded 3 days after seeding.

Images were acquired using the Live Acquisition 2.4 software of a 2000DC CCD digital camera (QImaging Retiga) mounted on a DM LFS Leica optical microscope equipped with a 20× objective water-immersion objective with Nomarski optics (see next subsection for details). Cell count was done with ImageJ software²⁶ by analyzing images taken from N2A cells grown on the SQIB:PCBM layers after three days of incubation (region of interest: 10 mm × 10 mm). The number of cells was normalized to the surface area for rough and smooth areas separately and averaged over four samples. Values are given as mean ± SEM.

Electrophysiological recordings and transient photocurrent measurements

All electrophysiological and transient photocurrent measurements were conducted on an upright DM LFS Leica microscope with a 20× water-immersion objective with Nomarski optics (Leica), comprising a polarizing microscope filter (Pol 513711 Leica/Leitz), a differential interference contrast (DIC) slider (D1 555063 Leica) and an analyser slider (L ICT/P 555045 Leica/Leitz).

The electrode consisted of an Ag/AgCl wire and a micropipette which was pulled from borosilicate glass (1.5 mm OD, Hilgenberg GmbH, Malsfeld, Germany) with a horizontal electrode puller (P97, Sutter, Novato, CA). The diameter of the pipette opening was typically around 1.5 μm. The Ag/AgCl wire was inserted, and the micropipette was filled with an

1
2
3 electrolyte solution, and the electrode resistance ranged from 3 to 6 M Ω . For transient
4 photocurrent measurements, electrodes were filled with Ringer's solution containing (in mM)
5 137 NaCl, 5.4 KCl, 1.8 CaCl₂, 1 MgCl₂, 10 D-glucose, and 5 HEPES (pH adjusted to 7.4
6 with 1 M NaOH). For whole-cell recordings of N2A cells, the intracellular solution contained
7 (in mM) 140 KCl, 1 CaCl₂, 2 MgCl₂, 11 EGTA, and 10 HEPES (pH adjusted to 7.4 with
8 1 M NaOH). Seal resistances of >1.5 G Ω were routinely obtained.
9

10
11 For both photocurrent and whole-cell transmembrane current recordings, the bath solu-
12 tion was always Ringer's solution and was kept at room temperature. The Ag/AgCl wire
13 was connected to a pipette holder (D = 1.5 mm, HEKA, Lambrecht, Germany), which was
14 further mounted to the HEKA headstage. A second Ag/AgCl wire which was also connected
15 to the headstage served as reference electrode within the electrolyte bath. Both Ag/AgCl
16 wires were regularly chlorinated with a 3 M FeCl₃ solution before the measurements. Cur-
17 rents were recorded with a HEKA EPC9 double patch-clamp amplifier at a sampling rate
18 of 25 kHz (whole-cell transmembrane recordings) and 20 kHz (photocurrent recordings) and
19 Bessel-filtered at 2.9 kHz with capacitance compensation of the electrode (C-fast) and the cell
20 membrane (C-slow) activated. Current-time curves were averaged over 10 single recordings.
21 Data were saved for offline analysis, which was done with Clampfit, Origin, or self-written
22 Matlab scripts.
23

24
25 The photoactive layer samples were placed at the bottom of the recording chamber with
26 the coated side facing upwards. Since they were not electrically contacted, they are referred
27 to as floating samples. The patch electrode was positioned in close proximity to the surface
28 (approximately 3 μ m), and the Ag/AgCl reference electrode in the bath solution closed the
29 electrical circuit. Thus, the flow of ions within the electrolyte only was measured upon
30 illumination of the photoactive layer. The amplifier software Patchmaster was in "set-up"
31 mode, i.e., no compensation modes were active. This rather unusual measurement protocol
32 for floating samples was adopted from Lanzani *et al.*¹¹. A sketch of our measurement setting
33 is provided in the Supporting Information Fig. S3.
34
35
36
37
38
39
40
41
42
43
44
45
46
47
48
49
50
51
52
53
54
55
56
57
58
59
60

1
2
3
4 A 150 W Xenon high stability lamp equipped with a monochromator (Polychrome V, Till
5 Photonics, Germany) and controlled by the Live Acquisition 2.4 software (Till Photonics)
6 served as light source. Furthermore, an optical UV/Vis quartz/quartz fibre (Till Photonics,
7 Germany) and a 90R/10 T beam splitter (400-700 nm, AHF, Germany) were used. The spec-
8 tral width of the monochromatic light was 15 nm at full width at half maximum. The samples
9 were irradiated through the 20 \times water-immersion objective of the microscope immersed into
10 the electrolyte. The intensity varied from 6 mW/mm² at 400 nm over 19 mW/mm² at 510 nm
11 to 8 mW/mm² at 690 nm. It was measured with a S170C low-power microscope slide power
12 meter sensor head immersed in Ringer's solution and a PM100D power meter (Thorlabs,
13 US). See Supporting Information Fig. S2 for intensity spectrum and corresponding photon
14 flux. Light pulses with square-wave shape had a duration of 10 ms with a latency of 290 ms
15 for stimuli trains consisting of 10 pulses.
16
17
18
19
20
21
22
23
24
25
26
27

28 For the TTX experiments, tetrodotoxin citrate (Cat. No. 1069) was purchased from
29 Tocris Bioscience. 100 μ L of a tetrodotoxin citrate solution in H₂O with a concentration of
30 1 mM was diluted with 100 mL Ringer's solution to give a concentration of 1 μ M. The TTX
31 was perfused into the bath solution by a pump (Ismatec, Wertheim, Germany).
32
33
34
35
36
37

38 **AFM and spatially resolved absorbance spectroscopy**

39
40 Atomic force microscopy (AFM, JPK NanoWizard) was performed under ambient conditions
41 in intermittent contact mode (Budget Sensors Tap-300G, resonance frequency 300 kHz, force
42 constant 40 N/m). In Ringer's solution a contact mode tip (NanoWorld Pointprobe CONT,
43 resonance frequency 13 kHz, force constant 0.2 N/m) was used in intermittent contact mode.
44
45 Samples were scanned twice a day over the course of one week with and without white-
46 light illumination from the 50 W microscope lamp (wavelength range 400 nm – 650 nm). By
47 occasionally scanning other parts of the sample it was ensured that the observed results
48 were no artifacts from repeated scanning. Spatially resolved optical absorbance spectra were
49 recorded using an Ocean Optics Maya spectrometer coupled to the camera port of an inverted
50
51
52
53
54
55
56
57
58
59
60

1
2
3 optical microscope (Nikon Eclipse TE 300) via a 200 μm optical fiber.
4
5
6

7 **EQE and total transmission measurements**

8

9
10 A Bentham PVE300 system was used, equipped with a dual Xenon/quartz halogen light
11 source, a Czerny-Turner TMc300 monochromator, and a DTR6 integrating sphere. The
12 spot size of the monochromatic light beam was set to 1.85 mm^2 . The intensity varied from
13 from 8 $\mu\text{W}/\text{mm}^2$ at 400 nm to 29 $\mu\text{W}/\text{mm}^2$ at 700 nm, measured with a S170C low-power
14 microscope slide power meter sensor head and a PM100D power meter (Thorlabs, US).
15
16 The total transmission was measured on dry samples with a spectral resolution of 1 nm
17 and the spectra were referenced to air. For the EQE measurements, the photoactive layer
18 was interfaced with Ringer's solution. The ITO layer was electrically contacted, as counter
19 electrode within the electrolyte a platinum wire was used. The monochromatic light with
20 5 nm wavelength resolution was modulated at 60 Hz. The data are referenced to illumination
21 intensity with a calibrated silicon solar cell using the data correction function of the BenWin+
22 software. The photocurrent was recorded under zero voltage bias conditions using a Stanford
23 Research SR830 lock-in amplifier after passing an AC-trans-impedance pre-amplifier set to
24 10^4 V/A gain.
25
26
27
28
29
30
31
32
33
34
35
36
37
38
39
40

41 **Results and Discussion**

42

43 **Photoactive layer characterization and compatibility to N2A cells**

44

45
46 The solution processed photoactive layer is supported on ITO-coated glass substrates and
47 consists of a 1:1 blend of the light-harvesting donor material SQIB and the fullerene accep-
48 tor PCBM, Fig. 1(a). The layer is thermally annealed at 180 $^\circ\text{C}$ under inert conditions for
49 2 h resulting in a birefringent, crystalline film with two distinct structural motifs, Fig. 1(b).
50 X-ray diffraction (XRD) investigations (not shown here) proof the crystalline nature of the
51 films and reveal the co-existence of the two different polymorphs of SQIB documented in
52
53
54
55
56
57
58
59
60

the literature²⁷ with a strong preferential out-of-plane orientation. Since XRD measurements do not provide spatial resolution, the structural motifs cannot be assigned to the polymorphs. However, this goes beyond the scope of the here presented work and will therefore be addressed elsewhere. The platelets consist of rotational domains with varying in-plane orientation, resulting in different intensities in a polarization microscope, Fig. 1(b). The detailed morphology and surface roughness is surveyed by atomic force microscopy, Fig. 1(c). The ferns are significantly rougher than the platelets with a root mean square roughness of $R_q = (55 \pm 8)$ nm. The voids between the fern structures are mostly covered by a 5 nm – 10 nm thick film, see also Supporting Information Fig. S1. This film consists most likely of PCBM, which remains amorphous, when SQIB phase-segregates from the blend upon crystallization. The roughness of the platelets varies with the amount of pinholes contained in the layer from $R_q = (2.5 \pm 0.6)$ nm for nearly pinhole-free areas to $R_q = (18 \pm 5)$ nm for areas with a large number of pinholes. The pinholes are elongated in shape, they are parallel within a single platelet domain, and orientation is rotated for different domains. They expose a surface, whose morphology resembles the one from ITO.

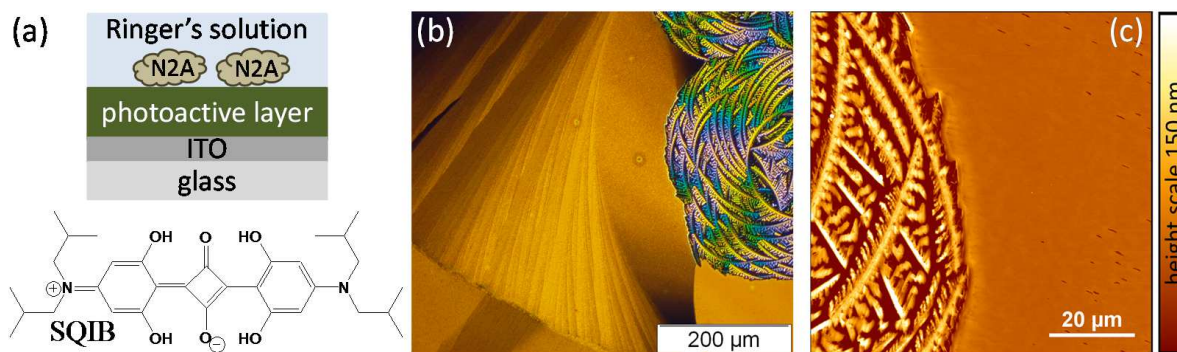


Figure 1: (a) Structural formula of the light-harvesting donor material SQIB. The sketch shows the sample arrangement for cultivation of N2A cells on the photoactive layer blend consisting of SQIB:PCBM (1:1) supported on ITO glass. (b) Polarized light microscopy image (Olympus BX41, crossed polarizers) of the photoactive layer shows two birefringent structural motifs referred to as (golden) platelets and (multicolored) ferns. (c) AFM identifies that the platelets are smooth while the ferns are comparatively rough. Elongated pinholes within the platelets are visible.

On the global level, the platelets usually cover the major part of the sample area. The

1
2
3 ferns cluster rather randomly on the sample area, making it possible to record UV/Vis ab-
4 sorbance spectra with varying shares of ferns within the spectrum by moving the illumination
5 spot over the surface. Absorbance spectra from different sample areas of 1.85 mm^2 covering
6 platelet-rich regions (black curve) as well as fern-rich regions (red curve) are graphed in
7 Fig. 2(a) with solid lines. The absorption of PCBM occurs mainly at lower wavelength and,
8 therefore, only a faint absorption tail is visible in the graph. Four peak positions are notice-
9 able within the spectra stemming from the SQIB: two humps located around 730 nm and
10 658 nm, and two shoulders located around 580 nm and 530 nm. The aspect ratio of the peaks
11 varies depending on the illumination spot position. For the platelet-rich region, the lowest
12 energy peak at 730 nm is more pronounced, while for the fern-rich region, the highest energy
13 shoulder at 530 nm becomes more distinct. Spatially resolved absorbance spectra have also
14 been recorded and are graphed in Fig. 2(a) with square or circle symbol lines. This allows to
15 assign specific spectral signatures to the two different structural motifs. The absorbance of
16 platelets (blue squares) is dominated by the lowest energy hump, while the spectrum of ferns
17 (yellow circles) peaks at the highest energy shoulder. The macroscopic absorbance results
18 from superposition of the local spectra of the two structural motifs, depending on their share
19 within the photoactive layer. The global spectrum can even be calculated as sum from the
20 resolved spectra of ferns and platelets, respectively, with different weighting factors.
21
22
23
24
25
26
27
28
29
30
31
32
33
34
35
36
37
38
39
40
41
42
43
44
45
46
47
48
49
50
51
52
53
54
55
56
57
58
59
60

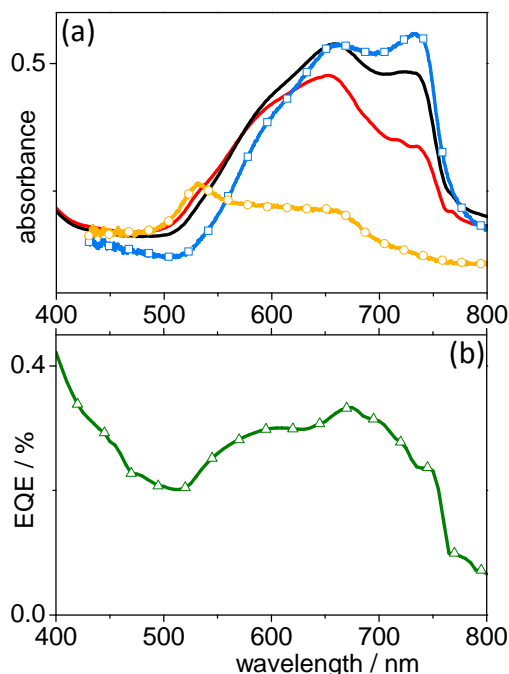


Figure 2: (a) Macroscopic and spatially resolved absorbance spectra of SQIB:PCBM photoactive layer blend: the solid lines correspond to a sample area of 1.85 mm^2 covering either a platelet-rich area (black) or a fern-rich area (red). The lines with symbols correspond to spatially resolved spectra of platelets (blue squares) and ferns (yellow circles). (b) EQE spectra show the spectral response of the photoactive layer blend interfaced with Ringer's solution (1.85 mm^2 spotsize) for illumination through the electrolyte (green triangles) with approximately equal platelet and fern contribution.

The photocurrent's spectral response from the SQIB:PCBM layer interfaced with Ringer's solution has been investigated by EQE measurements. Data are provided from samples irradiated through the electrolyte, Fig. 2(b), since this is the illumination direction used later on for the transient photocurrent and patch clamp recordings. At the photoconductor-electrolyte interface the conductance mode changes from (mainly) electronic to ionic. This can happen via electron transfer to the electrolyte (faradaic currents) and/or via a displacement (capacitive) current. The EQE measurement records the sum of both conductance modes. The EQE values are in general low, barely exceeding 0.4% at the maximum. The EQE spectrum resembles spectral absorbance signatures of the thin film. The comparatively large photocurrent at wavelengths below 500 nm can be attributed to free charge carrier generation within PCBM domains²⁸, while the photocurrent at higher wavelengths predom-

inantly stems from exciton splitting at SQIB:PCBM interfaces. However, the peak ratio of the two spectral humps stemming from SQIB is inverted compared to the absorbance of the corresponding thin film. The lowest energy hump, mainly associated with the platelet absorbance, dominates the photocurrent response. Such an antibatic resonance has also been documented for an ITO/P3HT/electrolyte junction, which is even more pronounced for that material system¹¹.

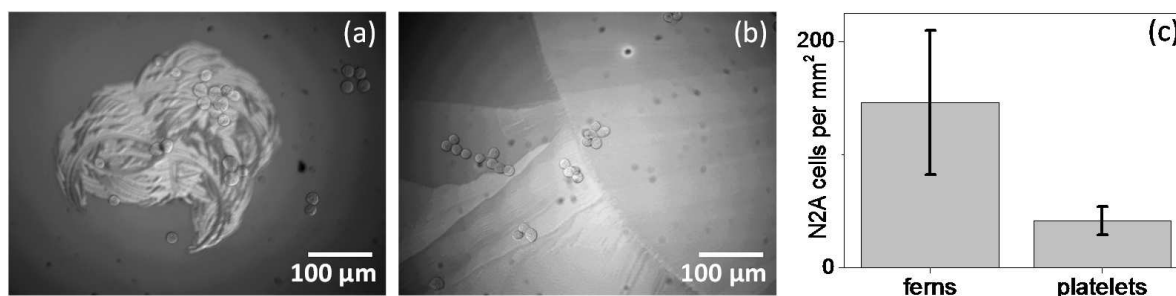
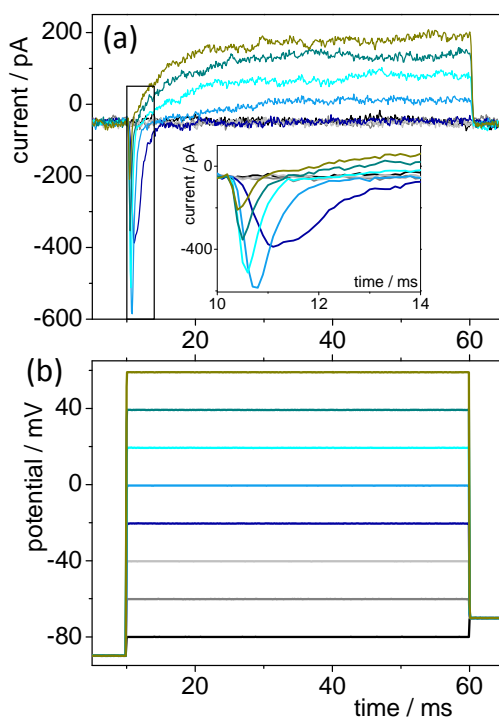


Figure 3: DIC microscopy image of N2A cells growing on (a) ferns and (b) platelets of the photoactive layer blend. (c) Quantitative analysis of the number density of N2A cells (density averaged over 4 samples, 31 regions of interest).

Having neuroelectronic applications in mind, good adhesion of neuronal cells to the active device area and non-impairment of cell viability plays a pivotal role. The pristine SQIB:PCBM photoactive layer blend fully supports adhesion and growth of N2A cells without any adhesion promoters. The cells have been seeded onto the photoactive layer and were cultivated for 3 days under physiological conditions prior to evaluation of their viability by optical microscopy, Fig. 3.

The number density of adhered, healthy cells was determined with respect to the structural motifs of the photoactive layer. The cells prefer the ferns for adhering with a density of roughly (150 ± 60) , and (40 ± 10) per square millimeter for the platelets, Fig. 3(c). Importantly, the good cell adhesion is achieved without an additional adhesion layer, such as the widely used poly-L-lysine. This is quite unusual because typically, smooth polymeric layers from, e.g., P3HT are non-sticky to neuronal cells^{11,12,29} while nanoscale-textured small molecular layers from, e.g., pentacene can support cell adhesion^{30,31}. Effort has been made

1
2
3
4 to increase adhesion properties by chemically binding lysin to a thiophene-based semicon-
5 ductor²³. However, the surface nanotopography has been found to be decisive instead of
6 its chemical composition^{32,33}. The nanotexture is, in turn, affecting surface tension and
7 wettability. Surfaces with moderate roughness from a few nanometers to a few ten nanome-
8 ters and with large fractal dimension promote adhesion by mimicking the complex disorder
9 of naturally occurring surfaces. Thus, the complex morphology of our photoactive layer is
10 beneficial for intimate interfacing with biological matter and promote cell survival.
11
12
13
14
15
16
17



41
42
43
44
45
46
47
48
49
50
51
52
53
54
55
56
57
58
59
60

Figure 4: Whole-cell patch-clamp recordings of N2A cells adhered to the photoactive layer in Ringer's solution. Cells were stimulated with rectangular-shaped depolarizing pulses. (a) Recordings of transmembrane current showed ionic inward and outward currents through sodium and potassium channels, respectively, for various depolarizing pulses (b). The inset in (a) shows a close-up of the initial sodium inward currents.

N2A cells naturally express voltage-gated sodium and potassium channels, whose functionality can be probed by electrophysiological patch-clamp recordings, Fig. 4. Depolarizing voltage steps, Fig. 4(b), induced fast sodium inward currents, visible as negative deflections in Fig. 4(a), inset shows a close-up, which were followed by slower potassium outward currents, visible as positive deflections, Fig. 4(a). Current time courses and amplitudes are

1
2
3 consistent with earlier reports on the native voltage-gated sodium and potassium channels
4 in N2A cells^{34,35}. Thus, these recordings provide evidence for the viability of N2A cells ad-
5 hered to the photoactive layer. Furthermore, they proved that the N2A cells can be used
6 as model system for monitoring an active response by opening of sodium channels to an
7 electrical stimulus.
8
9
10
11
12

13 **Photoactive layer stability investigation by AFM**

14
15
16 The stability of the photoconductor/electrolyte junction is essential for stable interfacing
17 with biological cells. The junction must also be stable under operation conditions, which
18 means under illumination in our case, since we consider photostimulation processes. There-
19 fore, SQIB:PCBM layers have been characterized by AFM in air, and immersed in Ringer's
20 solution with and without white light illumination (400 nm – 650 nm) from the top, respec-
21 tively. The upper row in Figure 5 shows images of the platelets under ambient conditions
22 (a), and in Ringer's solution after 3 days in dark (b), and after additional 3 days of constant
23 white light illumination (intensity 50 W/m²) (c). Cross sections along the same area (marked
24 by dashed colored lines in the AFM images) are presented in Figure 5(f). Placing the sample
25 in Ringer's solution leads to roughening, especially along cracks in the film, see Figure 5(b)
26 and the blue line in Figure 5(f). This trend is drastically accelerated by illumination with
27 white light, Figure 5(c) and the red line in Figure 5(f). The R_q roughness increases from
28 1.7 nm to 2.1 nm and 6.3 nm, respectively. A similar trend is observed for the ferns, Fig-
29 ure 5(d). Exposition for 6 days in total to Ringer's solution, the first 3 days in dark, and
30 the last 3 days under additional constant light illumination, leads to a loss of material and
31 to morphological changes. The ferns skeletonize, i.e., the veins are only slightly affected,
32 whereas for the leaf material is vanishing, Figures 5(e) and (g). However, since material
33 from the ferns is removed, the roughness R_q decreases from 63 nm to 28 nm.
34
35
36
37
38
39
40
41
42
43
44
45
46
47
48
49
50
51
52
53
54
55
56
57
58
59
60

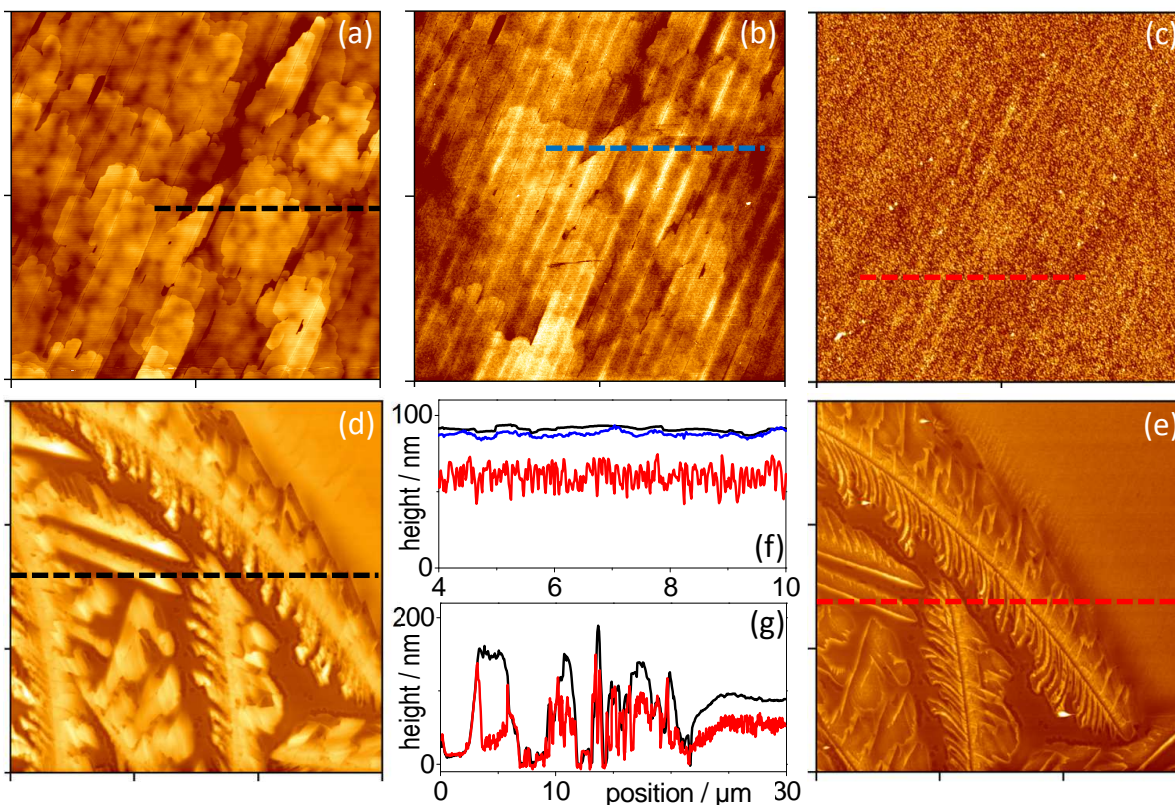
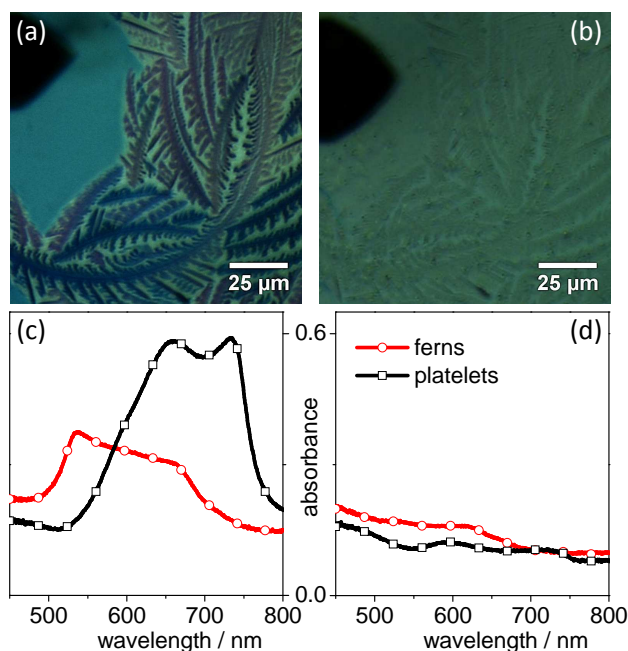


Figure 5: Morphological characterization of a SQIB:PCBM (1:1) blend film by AFM. Upper row ($10\ \mu\text{m} \times 10\ \mu\text{m}$): platelets under (a) ambient conditions, (b) in Ringer's solution after 3 days, and (c) in Ringer's solution after additional 3 days of constant illumination. Lower row ($30\ \mu\text{m} \times 30\ \mu\text{m}$): ferns under ambient conditions (d), and in Ringer's solution (e) after 6 days with additional constant white illumination for the last 3 days. Height scales are 8 nm (a), 10 nm (b), 30 nm (c), and 280 nm (d) and (e). Cross sections along the same sample area (dashed lines) are shown in (f) for the upper row and in (g) for the lower row.

Optical microscope images before and after illumination with light in Ringer's solution are shown in Figures 6(a) and (b), respectively. Here, the sample is illuminated with linear polarized light. Since the photoactive layers are dichroic and birefringent, colors are observed depending on the orientation of the molecules within the structures. For unpolarized illumination, the platelets also appear blue-green, whereas the ferns are dark colored (not shown here). The brighter areas in between the ferns most likely correspond to dewetted ITO or PCBM on ITO. After white light illumination for three days in Ringer's solution, the colors of both the smooth and rough areas have faded out, Figure 6(b). The colors for unpolarized illumination are reflected in the absorbance spectra, Figure 6(c). Note that the

1
2
3 spectra were referenced to the glass substrate and, therefore, include the contribution from
4 ITO. The loss of SQIB material is clearly noticeable by the reduction in absorbance. The
5 spectral range from 450 nm to 800 nm, which was chosen according to the limitations of the
6 optical components, does not include the absorption of the PCBM share within the layer.
7 Thus, it remains unclear, if the PCBM stays on the surface and only SQIB is removed.
8
9
10
11
12
13



35
36
37
38
39
40
41
42
43
44
45
46
47
48
49
50
51
52
53
54
55
56
57
58
59
60

Figure 6: Polarized microscopy images of platelets and ferns of a SQIB:PCBM layer before (a) and after (b) illumination in Ringer's solution. The dark triangular spot in the upper left corner is the AFM cantilever. In (c) and (d) absorption spectra (reference glass) before and after illumination are displayed for the ferns (red circles) and platelets (black squares) are presented, respectively.

Other small molecular semiconductors, such as pentacene³¹, or polymeric materials such as P3HT²⁹ have been shown to be stable upon exposure to physiological electrolytes and to tolerate cell culturing. However, illuminated conditions or other operation conditions, such as voltage biasing, have only been addressed rarely. Pristine P3HT films have been demonstrated to undergo a reversible reaction with molecular oxygen under ambient conditions, and when interfaced with saline solutions³⁶. Illumination enhanced the process, but no ablation of material was noticed, and the samples could even be healed by re-annealing under inert conditions. It was concluded, that interfacing with saline solutions was at least not

1
2
3 worse than exposure to ambient conditions. This is analog to our findings. In control exper-
4 iments (not shown here) on illuminated SQIB:PCBM samples under ambient air conditions,
5 or interfaced with DI water, a similar photo-ablation process was noticed as upon interfacing
6 with Ringer's solution. The PCBM could function as a catalyst for the photo-degradation,
7 due to its electron accepting nature, and promote oxidation and fragmentation of the SQIB.
8 However, the long-lasting stability under dark conditions assures that the system is also
9 stable during cell culturing, and the slow degradation under illumination allows to conduct
10 reproducible photoelectrical measurements.
11
12
13
14
15
16
17
18
19
20

21 **Transient photocurrent measurements and patch-clamp recordings**

22
23
24 The local transient photocurrent response of floating SQIB:PCBM samples immersed in
25 Ringers's solution was recorded by positioning a patch-clamp electrode in close proximity
26 above either a platelet or a fern region. The electrical circuit was closed by a Ag/AgCl
27 electrode inserted into the electrolyte bath. The samples were illuminated with trains of
28 10 ms long, square-wave shaped, narrow-band (15 nm bandwidth), light pulses from the top
29 through the Ringer's solution. Note that the illumination spot was larger than the mouth
30 of the patch-clamp electrode, and the active area of the photoconductor/electrolyte junction
31 is not defined, thus no current density but absolute, baseline-corrected current values are
32 displayed. The dependence of the photocurrent on illumination intensity is shown in the
33 Supporting Information in Figs. S4 and S5. In Figs. 7(a)-(c) the photocurrent is graphed
34 for three different values of excitation wavelength, above a platelet region (black curves) and
35 above a fern region (red curves). A more detailed presentation of the spectral response of the
36 transient current peaks is given in the Supporting Information Fig. S6. For both light ON and
37 OFF, the photocurrent showed a transient peak with different polarity, and a significantly
38 smaller, positive steady-state photocurrent. In general, the response was stronger, rising to
39 higher peak-current values and steady-state currents, for the platelet region. This trend fits
40 in with the EQE measurements. The ON transients always had a positive polarity, while the
41
42
43
44
45
46
47
48
49
50
51
52
53
54
55
56
57
58
59
60

1
2
3 OFF transients were of reversed, negative polarity. Depending on the excitation wavelength,
4
5 the ON transients consisted of a double peak. The first ON peak was always stronger than
6
7 the second ON peak, which was noticeable from 530 nm illumination onwards to 690 nm. The
8
9 steady-state current is faint compared to the transient current. We consider it as negligibly
10
11 since it is not relevant for the capacitive coupling mechanism to stimulate neuronal cells.
12

13
14 The transient photocurrent can be explained by a capacitive displacement current without
15
16 charge transfer across the semiconductor-electrolyte interface²⁴. Photogenerated charge car-
17
18 riers form a space charge region within the semiconductor accumulate at the semiconductor-
19
20 electrolyte interface. The dissolved ions within the electrolyte are mobile and rapidly form
21
22 a Helmholtz electric double layer at the electrolyte-semiconductor interface. The type of
23
24 charge carriers, i.e., positive holes or negative electrons, accumulating at the interface deter-
25
26 mines the polarity of the photocurrent. This is in turn influenced by, e.g., the thickness of
27
28 the photoactive layer and the direction of illumination³⁷, the excitation wavelength³⁸, blend
29
30 composition, and choice of electrode and electrolyte or solid dielectric layer³⁹. The magni-
31
32 tude of the transient current peak depends on the photoconductor's spectral responsivity
33
34 and the illumination intensity, as well as the dielectric properties of the electrolyte²⁴. A
35
36 double-peak nature of the ON transient, as in our case, has not been documented before.
37
38 Albeit Awaga *et al.*³⁹ noted a double peak for a specific composition of a P3HT:PCBM blend
39
40 in contact with an ionic liquid, this were two peaks of opposite polarity. This was attributed
41
42 to a consecutive change of the type of accumulating charge carriers, i.e. accumulation of
43
44 electrons followed by accumulation of holes or vice versa. In our case, the two consecutive
45
46 peaks are of the same polarity, meaning accumulation of the same type of charge carriers,
47
48 but with a different dynamic behavior. The control experiments on neat and blended films
49
50 presented in the Supporting Information in Fig. S7 hint to that. However, the origin remains
51
52 elusive, and its discussion goes beyond the scope of the present study, and hence will be part
53
54 of future studies. Typically, the transients show a single exponential rise and a double expo-
55
56 nential decay when using ionic liquids as dielectric layer³⁹. The time constants of the decay
57
58
59
60

function are determined by the capacitance of the dielectric layer, they increase with increasing insulating layer capacitance⁴⁰. A small leakage steady-state current during illumination can drain the accumulated charges, so that the discharging current, i.e., the OFF transient current of opposite polarity is decreased in magnitude compared to the ON transient. When a redox-active mediator within an electrolyte enforces charge transfer across the interface, the transient current peak is quenched in favor of a steady-state current³⁷.

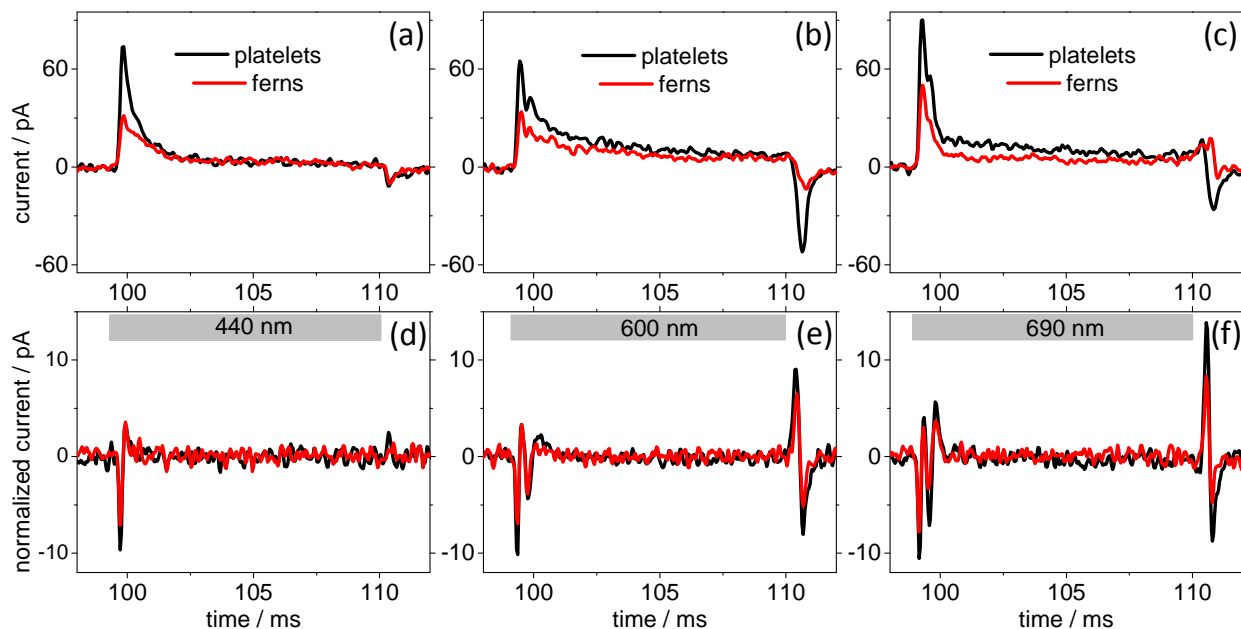


Figure 7: Upper row: transient photocurrents of floating SQIB:PCBM samples in Ringers's solution. The patch-pipette was positioned above either a platelet region (black curves) or a fern region (red curves). Lower row: whole-cell transmembrane currents recorded in voltage clamp mode of N2A cells adhering on the photoactive layer. The holding potential was at -70 mV. To account for differences in cell size and membrane surface, current values were normalized to 10 pF capacitance. The black curves indicate N2A cells adhered on platelets, while the red curves indicate cells on ferns. The length of the light pulses was 10 ms in all cases, the grey bar is graphed for illustrating the illumination period. The excitation was centered at 440 nm for (a) and (d), at 600 nm for (b) and (e), and at 690 nm for (c) and (f).

Transmembrane currents were recorded in whole-cell configuration from N2A cells grown on the photoconductor and are shown in Fig. 7(d)-(f) for three selected excitation wavelength values. The current values were baseline corrected and normalized to 10 pF membrane capacitance to account for differences in cell size. The voltage was clamped at -70 mV. The cells responded to the ON and OFF transients arising from the photoconductor junction upon

1
2
3 illumination with rapid transmembrane currents. The cells were either adhered to platelet
4 regions (black curves), resulting in a slightly stronger current, or to fern regions (red curves)
5 of the photoconductor. The double-peak nature of the photocurrent transients starting from
6 530 nm illumination onwards to longer wavelength was also conserved. This clearly indi-
7 cated an intimate contact between cell and photoconductor allowing direct, fast and highly
8 resolved signal transfer across the junction. According to the Hodgkin-Huxley model⁴¹ such
9 a rapid transmembrane current can be interpreted as capacitive current: $I_{cM} = c_M \cdot \frac{dV_M}{dt}$
10 with V_M being the membrane potential and c_M being the membrane capacitance. Such a
11 capacitive current is classified as a passive response of the cell. It is caused by a change
12 in membrane potential, either a hyperpolarization (decrease in potential) or a depolariza-
13 tion (increase in potential), deciding on the polarity of the capacitive current. Note that the
14 membrane potential is referred to the inside of a cell, which is typically negative with respect
15 to the outside. Fig. 8(b) exemplarily shows the membrane potential of an N2A cell recorded
16 in current clamp mode for illumination of the underlying photoconductor at 690 nm. The
17 resting potential of the cell was around $V_M = -75$ mV. Upon turning the red light on, the
18 membrane potential showed two rapid depolarizations in the order $\Delta V_M = 0.4$ mV. When
19 the light was turned off, a single, rapid hyperpolarization became visible.
20
21
22
23
24
25
26
27
28
29
30
31
32
33
34
35
36
37
38
39
40
41
42
43
44
45
46
47
48
49
50
51
52
53
54
55
56
57
58
59
60

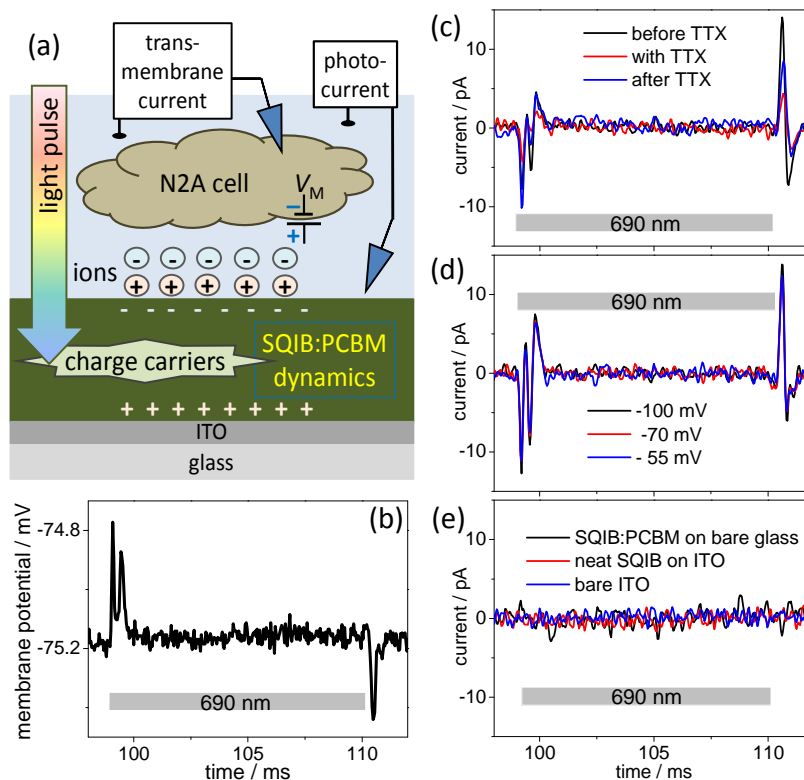


Figure 8: (a) The sketch pictures the experimental setting for transient photocurrent as well as patch-clamp recordings, and illustrates the movement of charge carriers causing the transient photocurrent and the subsequent depolarization of the cell membrane. (b) Membrane potential of N2A cell stimulated by the transient photocurrent, recorded in current clamp mode. Righthand: Whole-cell transmembrane currents normalized to 10 pF of N2A cell recorded in voltage clamp mode, stimulated by transient photocurrents: (c) TTX control experiment, (d) variation of holding potential as indicated, (e) variation of photoconductor architecture. Illumination was through the Ringers's solution with 10 ms pulses centered at 690 nm in all cases.

We propose an accumulation of negative charge carriers at the photoconductor-electrolyte interface, when the light is turned on, Fig. 8(a). This causes positive ions to drift within the electrolyte to the interface forming a Helmholtz double layer. As a consequence, the outside of the cell membrane above the photoconductor becomes negative, which is then, in turn, probed as depolarization. Note that the depolarization pulse here is *extracellular*, while typical voltage protocols for patch-clamp recordings utilize *intracellular* depolarizing pulses. Ion movement, i.e., transient photocurrent, and resulting depolarization are short lasting events. The photoconductor-electrolyte junction stays, apart from some leakage current, in the ex-

1
2
3
4 cited state during the illumination, while the cell membrane returns to its resting potential.
5
6 When the light is turned off, the charge carriers within the photoactive layer recombine, and
7
8 the drift of ions within the electrolyte is reversed, resulting in a rapid hyperpolarization of
9
10 the cell membrane. In general, a depolarization can induce opening of voltage-gated sodium
11
12 ion channels, if a certain threshold potential is overcome. The extent of depolarization ΔV_M
13
14 in our case was very small, less than half a millivolt. This value is not likely to overcome
15
16 the threshold for the opening of voltage-gated sodium channels. The resulting ionic trans-
17
18 membrane currents would be noticeable as a slow event in the patch-clamp recordings, see
19
20 Fig. 4, which was not the case for our studies. We have altered the holding potential for
21
22 the voltage-clamp recordings in order to approach the threshold voltage, but the stimulated
23
24 change in membrane potential was too small. According to standard measurements with a
25
26 set of intracellular depolarizing pulses, see Fig. 4, the membrane potential V_M must be raised
27
28 to approximately -20 mV corresponding to a change in membrane potential ΔV_M of a few
29
30 tens of millivolts. Thus, we could not evidence the anticipated active response of the N2A
31
32 cell to a light-triggered stimulus from the photoconductor-electrolyte junction for the given
33
34 experimental parameters.
35

36
37 However, we wanted to be sure about the bare capacitive nature of the recorded trans-
38
39 membrane currents, so we performed three control experiments in which N2A cells were
40
41 directly adhered to the photoactive layer: 1) The sodium channels were inactivated with
42
43 TTX⁴², Fig. 8(c), and 2) the holding potential was varied to more negative values for volt-
44
45 age clamp recordings to exclude all ionic currents⁴³, Fig. 8(d). In both experiments, the rapid
46
47 transmembrane currents remained unchanged, confirming that they were of pure capacitive
48
49 nature. 3) We wanted to exclude effects other than photoelectrical, such as photothermal
50
51 effects, which recently emerged as hot topic for organic artificial photoreceptors¹³. There-
52
53 fore, we altered the device architecture by depositing the SQIB:PCBM blend on bare glass
54
55 substrates and a neat SQIB layer on ITO substrates. For clarity, we also grew N2A cells on
56
57 bare ITO substrates. Patch-clamp recordings on the N2A cells did not show any response
58
59
60

1
2
3
4 in these cases, Fig. 8(e). In summary, these control experiments demonstrate that the rapid
5
6 transmembrane currents indeed represent capacitive currents.

7
8 It has already been demonstrated in the literature by Lanzani *et al.*¹⁰ and Narayan
9
10 *et al.*^{11,12}, that organic photoconductor electrolyte junctions could trigger neuronal firing
11
12 in primary cultures of hippocampal neurons, as well as in explanted degenerated retinas.
13
14 The mechanism was assumed to be of photo*electrical* nature according to pioneering work
15
16 Fromherz *et al.*⁴²⁻⁴⁴ on purely electrical stimulation of sodium and potassium ion channels
17
18 in HEK cells cultured on silicon chips. Fromherz *et al.* clearly evidenced and modeled a
19
20 capacitive coupling mechanism from an oxide-coated silicon chip biased with a voltage ramp
21
22 through an electrolyte to the adhered cell. The coupling strength was determined by the
23
24 capacitance of the chip and the conductance of the electrolyte, thus by the *RC* constant of
25
26 the chip-electrolyte junction. In order to facilitate opening of ion channels, the *RC* constant
27
28 was increased by decreasing the conductance of the electrolyte, meaning that the electrolyte
29
30 was no longer physiological. Also note that for growing the cells on the chip, a polymeric
31
32 adhesion layer was required, which was not included in the modeling. Recently, Antognazza
33
34 *et al.*¹³ revised the coupling mechanism from the organic photoconductor electrolyte junction
35
36 and found a photo*thermal* mechanism to be more likely under physiological conditions. The
37
38 light pulses employed for photo-excitation were 200 ms long, thus 20 times longer than our
39
40 light pulses, resulting in a sizable temperature increase. The authors documented that the
41
42 ion channels were activated by a temperature-induced change in membrane capacitance,
43
44 while electrical coupling induced a passive response of the cell by capacitive transmembrane
45
46 currents only. These results are very similar to our findings showing that the electrical
47
48 capacitive coupling was on one hand highly effective, but on the other hand not able to
49
50 activate ionic conductance through the cell membrane. A heating effect was avoided in our
51
52 case by using substantially shorter light pulses. Note that, different from the other group's
53
54 work, we did not employ an adhesion layer for growing cells, which might alter the situation.
55
56 Therefore, applying biological adhesion layers or other dielectric coatings of the active layer
57
58
59
60

1
2
3 will be part of future studies.
4
5
6

7 8 Conclusions

9
10
11 In the present study, we have demonstrated a fast and direct capacitive coupling between
12 N2A cells and a small molecular semiconductor / physiological electrolyte junction. Our
13 squaraine-based active layer exhibited a unique textured morphology, which was beneficial
14 for cell adhesion and did not impair cell viability, even without the use of an adhesion layer.
15 The stability of the photoconductor layer in physiological electrolyte environment, monitored
16 by atomic force microscopy, was also sufficient. Patch-clamp recordings showed that photo-
17 induced transient displacement currents at the organic semiconductor-electrolyte interface
18 stimulated fast capacitive transmembrane currents in N2A cells. We could not observe the
19 anticipated active response of the cells via ionic conductance through the cell membrane, i.e.,
20 opening of ion channels. Thermal effects have been excluded by using short light pulses for
21 the photostimulation. Similar organic polymer-based electrolyte junctions have been demon-
22 strated by others to trigger active responses of neuronal cells via a photothermal coupling
23 mechanism upon photo-excitation with significantly longer light pulses. We conclude that
24 the electrical coupling alone was not able to activate voltage-gated ion channels in N2A cells.
25 In future studies, we will concentrate on further investigation of the coupling mechanism,
26 considering thermal effects and dielectric properties of adhesion layers. We see a large future
27 potential in organic-based artificial photoreceptors for retinal prosthetic devices. It is now
28 of major importance to conduct mechanistic studies on a model system to understand the
29 mutual requirements of organic electronics and living cells or tissue. This will pave the way
30 for targeted development of novel, organic-based neuroprosthetics for vision restoration.
31
32
33
34
35
36
37
38
39
40
41
42
43
44
45
46
47
48
49
50
51
52
53
54
55
56
57
58
59
60

Acknowledgement

The authors thank Susanne Wallenstein and Nicole Iben for excellent technical assistance on the cell culturing, and Matthias Macke for practical support. OSA thanks the DFG for a scholarship within the research training group Molecular Basis of Sensory Biology GRK 1885/1.

Supporting Information Available

AFM images; microscope lamp characterization; sketch of experimental setup for transient photocurrent measurements; illumination intensity dependent and spectrally resolved transient photocurrent of neat and blended films interfaced with physiological electrolyte. This material is available free of charge via the Internet at <http://pubs.acs.org/>.

References

- (1) Fromherz, P. Three levels of neuroelectronic interfacing. *Ann. N.Y. Acad. Sci.* **2006**, *1093*, 143–160.
- (2) Berggren, M.; Richter-Dahlfors, A. Organic bioelectronics. *Adv. Mater.* **2007**, *19*, 3201–3213.
- (3) Irimia-Vladu, M. Green electronics: biodegradable and biocompatible materials and devices for sustainable future. *Chem. Soc. Rev.* **2014**, *43*, 588–610.
- (4) Cramer, T.; Campana, A.; Leonardi, F.; Casalini, S.; Kyndiah, A.; Murgia, M.; Biscarini, F. Water-gated organic field effect transistors—opportunities for biochemical sensing and extracellular signal transduction. *J. Mater. Chem. B* **2013**, *1*, 3728–3741.
- (5) Bareket-Keren, L.; Hanein, Y. Novel interfaces for light directed neuronal stimulation: advances and challenges. *Int. J. Nanomedicine* **2014**, *9*, 65–83.

- 1
2
3
4 (6) Hadjinicolaou, A. E.; Meffin, H.; Maturana, M. I.; Cloherty, S. L.; Ibbotson, M. R.
5 Prosthetic vision: devices, patient outcomes and retinal research. *Clin. Exp. Optom.*
6 **2015**, *98*, 395–410.
7
8
9
10 (7) Chernov, I.; Greb, H.; Janssen-Bienhold, U.; Parisi, J.; Weiler, R.; von Hauff, E. Binding
11 and potential-triggered release of l-glutamate with molecularly imprinted polypyrrole
12 in neutral pH solutions. *Sensors and Actuators B: Chemical* **2014**, *203*, 327–332.
13
14
15
16
17 (8) Broichhagen, J.; Damijonaitis, A.; Levitz, J.; Sokol, K. R.; Leippe, P.; Konrad, D.;
18 Isacoff, E. Y.; Trauner, D. Orthogonal Optical Control of a G Protein-Coupled Receptor
19 with a SNAP-Tethered Photochromic Ligand. *ACS Cent. Sci.* **2015**, *1*, 383–393.
20
21
22
23
24 (9) Laprell, L.; Hu ll, K.; Stawski, P.; Schön, C.; Michalakis, S.; Biel, M.; Sumser, M. P.;
25 Trauner, D. Restoring light sensitivity in blind retinae using a photochromic AMPA
26 receptor agonist. *ACS Chem. Neurosci.* **2016**, *7*, 15–20.
27
28
29
30
31 (10) Ghezzi, D.; Antognazza, M. R.; Dal Maschio, M.; Lanzarini, E.; Benfenati, F.; Lan-
32 zani, G. A hybrid bioorganic interface for neuronal photoactivation. *Nat. Commun.*
33 **2011**, *2*, 166.
34
35
36
37
38 (11) Ghezzi, D.; Antognazza, M. R.; Maccarone, R.; Bellani, S.; Lanzarini, E.; Martino, N.;
39 Mete, M.; Pertile, G.; Bisti, S.; Lanzani, G.; Benfenati, F. A polymer optoelectronic
40 interface restores light sensitivity in blind rat retinas. *Nat. Photonics* **2013**, *7*, 400–406.
41
42
43
44
45 (12) Gautam, V.; Rand, D.; Hanein, Y.; Narayan, K. A polymer optoelectronic interface
46 provides visual cues to a blind retina. *Adv. Mater.* **2014**, *26*, 1751–1756.
47
48
49
50 (13) Martino, N.; Feyen, P.; Porro, M.; Bossio, C.; Zucchetti, E.; Ghezzi, D.; Benfenati, F.;
51 Lanzani, G.; Antognazza, M. R. Photothermal cellular stimulation in functional bio-
52 polymer interfaces. *Sci. Rep.* **2015**, *5*, 8911.
53
54
55
56
57
58
59
60

- 1
2
3
4
5
6
7
8
9
10
11
12
13
14
15
16
17
18
19
20
21
22
23
24
25
26
27
28
29
30
31
32
33
34
35
36
37
38
39
40
41
42
43
44
45
46
47
48
49
50
51
52
53
54
55
56
57
58
59
60
- (14) Fattahi, P.; Yang, G.; Kim, G.; Abidian, M. R. A review of organic and inorganic biomaterials for neural interfaces. *Adv. Mater.* **2014**, *26*, 1846–1885.
- (15) Rivnay, J.; Owens, R. M.; Malliaras, G. G. The rise of organic bioelectronics. *Chem. Mater.* **2013**, *26*, 679–685.
- (16) Hestand, N. J.; Zheng, C.; Penmetcha, A. R.; Cona, B.; Cody, J. A.; Spano, F. C.; Collison, C. J. Confirmation of the Origins of Panchromatic Spectra in Squaraine Thin Films Targeted for Organic Photovoltaic Devices. *J. Phys. Chem. C* **2015**, *119*, 18964–18974.
- (17) Halton, B. From Small Rings to Big Things: Xerography, Sensors, and the Squaraines. *Chem. New Zealand* **2008**, *72*, 57.
- (18) Chen, G.; Sasabe, H.; Igarashi, T.; Hong, Z.; Kido, J. Squaraine Dyes for Organic Photovoltaic Cells. *J. Mater. Chem. A* **2015**, *3*, 14517–14534.
- (19) Jiang, J.-Q.; Sun, C.-L.; Shi, Z.-F.; Zhang, H.-L. Squaraines as light-capturing materials in photovoltaic cells. *RSC Adv.* **2014**, *4*, 32987–32996.
- (20) Brück, S.; Krause, C.; Turrisi, R.; Beverina, L.; Wilken, S.; Saak, W.; Lützen, A.; Borchert, H.; Schiek, M.; Parisi, J. Structure–property relationship of anilino-squaraines in organic solar cells. *Phys. Chem. Chem. Phys.* **2014**, *16*, 1067–1077.
- (21) Beverina, L.; Salice, P. Squaraine compounds: tailored design and synthesis towards a variety of material science applications. *Eur. J. Org. Chem.* **2010**, *2010*, 1207–1225.
- (22) Beverina, L.; Sassi, M. Twists and Turns Around a Square: The Many Faces of Squaraine Chemistry. *Synlett* **2014**, *25*, 477–490.
- (23) Bonetti, S.; Pistone, A.; Brucale, M.; Karges, S.; Favaretto, L.; Zambianchi, M.; Posati, T.; Sagnella, A.; Caprini, M.; Toffanin, S.; Zamboni, R.; Camaioni, N.; Muccini, M.; Melucci, M.; Benfenati, V. A Lysinated Thiophene-Based Semiconductor as

- 1
2
3 a Multifunctional Neural Bioorganic Interface. *Adv. Healthcare Mater.* **2015**, *4*, 1190–
4 1202.
5
6
7
8
9 (24) Hu, L.; Liu, X.; Dalglish, S.; Matsushita, M. M.; Yoshikawa, H.; Awaga, K. Organic
10 optoelectronic interfaces with anomalous transient photocurrent. *J. Mater. Chem. C*
11 **2015**, *3*, 5122–5135.
12
13
14
15 (25) Tian, M.; Furuki, M.; Iwasa, I.; Sato, Y.; Pu, L. S.; Tatsuura, S. Search for squaraine
16 derivatives that can be sublimed without thermal decomposition. *J. Phys. Chem. B*
17 **2002**, *106*, 4370–4376.
18
19
20
21
22 (26) Rasband, W. ImageJ. 1997 – 2016; <http://imagej.nih.gov/ij/>.
23
24
25 (27) Viterisi, A.; Montcada, N. F.; Kumar, C. V.; Gispert-Guirado, F.; Martin, E.; Escud-
26 ero, E.; Palomares, E. Unambiguous determination of molecular packing in crystalline
27 donor domains of small molecule solution processed solar cell devices using routine
28 X-ray diffraction techniques. *J. Mater. Chem. A* **2014**, *2*, 3536–3542.
29
30
31
32
33 (28) Burkhard, G. F.; Hoke, E. T.; Beiley, Z. M.; McGehee, M. D. Free carrier generation
34 in fullerene acceptors and its effect on polymer photovoltaics. *J. Phys. Chem. C* **2012**,
35 *116*, 26674–26678.
36
37
38
39
40 (29) Scarpa, G.; Idzko, A.-L.; Götz, S.; Thalhammer, S. Biocompatibility Studies of
41 Functionalized Regioregular Poly (3-hexylthiophene) Layers for Sensing Applications.
42 *Macromol. Biosci.* **2010**, *10*, 378–383.
43
44
45
46
47 (30) Tonazzini, I.; Bystrenova, E.; Chelli, B.; Greco, P.; Stoliar, P.; Calò, A.; Lazar, A.;
48 Borgatti, F.; D'Angelo, P.; Martini, C.; Biscarini, F. Multiscale morphology of organic
49 semiconductor thin films controls the adhesion and viability of human neural cells.
50 *Biophys. J.* **2010**, *98*, 2804–2812.
51
52
53
54
55
56
57
58
59
60

- 1
2
3
4
5
6
7
8
9
10
11
12
13
14
15
16
17
18
19
20
21
22
23
24
25
26
27
28
29
30
31
32
33
34
35
36
37
38
39
40
41
42
43
44
45
46
47
48
49
50
51
52
53
54
55
56
57
58
59
60
- (31) Bystrenova, E.; Jelitai, M.; Tonazzini, I.; N Lazar, A.; Huth, M.; Stoliar, P.; Dionigi, C.; Cacace, M. G.; Nickel, B.; Madarasz, E.; Biscarini, F. Neural networks grown on organic semiconductors. *Adv. Funct. Mater.* **2008**, *18*, 1751–1756.
- (32) Gentile, F.; Tirinato, L.; Battista, E.; Causa, F.; Liberale, C.; di Fabrizio, E. M.; Decuzzi, P. Cells preferentially grow on rough substrates. *Biomaterials* **2010**, *31*, 7205–7212.
- (33) Anselme, K.; Davidson, P.; Popa, A.; Giazzon, M.; Liley, M.; Ploux, L. The interaction of cells and bacteria with surfaces structured at the nanometre scale. *Acta Biomater.* **2010**, *6*, 3824–3846.
- (34) Chao, C.-C.; Shieh, J.; Kuo, S.-C.; Wu, B.-T.; Hour, M.-J.; Leung, Y.-M. HMJ-53A accelerates slow inactivation gating of voltage-gated K⁺ channels in mouse neuroblastoma N2A cells. *Neuropharmacol.* **2008**, *54*, 1128–1135.
- (35) Combs, D. J.; Shin, H.-G.; Xu, Y.; Ramu, Y.; Lu, Z. Tuning voltage-gated channel activity and cellular excitability with a sphingomyelinase. *J. Gen. Physiol.* **2013**, *142*, 367–380.
- (36) Bellani, S.; Fazzi, D.; Bruno, P.; Giussani, E.; Canesi, E. V.; Lanzani, G.; Antognazza, M. R. Reversible P3HT/Oxygen Charge Transfer Complex Identification in Thin Films Exposed to Direct Contact with Water. *J. Phys. Chem. C* **2014**, *118*, 6291–6299.
- (37) Gautam, V.; Bag, M.; Narayan, K. Dynamics of bulk polymer heterostructure/electrolyte devices. *J. Phys. Chem. Lett.* **2010**, *1*, 3277–3282.
- (38) Gautam, V.; Bag, M.; Narayan, K. Single-pixel, single-layer polymer device as a tricolor sensor with signals mimicking natural photoreceptors. *J. Am. Chem. Soc.* **2011**, *133*, 17942–17949.

- 1
2
3
4 (39) Reissig, L.; Mori, K.; Treadwell, R.; Dalglish, S.; Awaga, K. Factors affecting the
5 polarity and magnitude of photoresponse of transient photodetectors. *Phys. Chem.*
6 *Chem. Phys.* **2016**, *18*, 6821–6830.
7
8
9
10 (40) Reissig, L.; Dalglish, S.; Awaga, K. A differential photodetector: Detecting light mod-
11 ulations using transient photocurrents. *AIP Adv.* **2016**, *6*, 015306.
12
13
14
15 (41) Hodgkin, A.; Huxley, A. A quantitative description of membrane current and its appli-
16 cation to conduction and excitation in nerve. *Bull. Math. Biol.* **1990**, *52*, 25–71.
17
18
19
20 (42) Schoen, I.; Fromherz, P. Activation of Na⁺ channels in cell membrane by capacitive
21 stimulation with silicon chip. *Appl. Phys. Lett.* **2005**, *87*, 193901.
22
23
24
25 (43) Schoen, I.; Fromherz, P. The mechanism of extracellular stimulation of nerve cells on
26 an electrolyte-oxide-semiconductor capacitor. *Biophys. J.* **2007**, *92*, 1096–1111.
27
28
29
30 (44) Ulbrich, M.; Fromherz, P. Opening of K⁺ channels by capacitive stimulation from silicon
31 chip. *Appl. Phys. A* **2005**, *81*, 887–891.
32
33
34
35
36
37
38
39
40
41
42
43
44
45
46
47
48
49
50
51
52
53
54
55
56
57
58
59
60

Graphical TOC Entry

